

RESEARCH ARTICLE

Open Access



# Computational spectropolarimetry with a tunable liquid crystal metasurface

Yibo Ni, Chen Chen, Shun Wen, Xinyuan Xue, Liqun Sun and Yuanmu Yang\*

## Abstract

While conventional photodetectors can only measure light intensity, the vectorial light field contains much richer information, including polarization and spectrum, that are essential for numerous applications ranging from imaging to telecommunication. However, the simultaneous measurement of multi-dimensional light field information typically requires the multiplexing of dispersive or polarization-selective elements, leading to excessive system complexity. Here, we demonstrate a near-infrared spectropolarimeter based on an electrically-tunable liquid crystal metasurface. The tunable metasurface, which acts as an encoder of the vectorial light field, is tailored to support high-quality-factor guided-mode resonances with diverse and anisotropic spectral features, thus allowing the full Stokes parameters and the spectrum of the incident light to be computationally reconstructed with high fidelity. The concept of using a tunable metasurface for multi-dimensional light field encoding may open up new horizons for developing vectorial light field sensors with minimized size, weight, cost, and complexity.

**Keywords:** Tunable metasurface, Liquid crystal, Computational spectropolarimetry

## 1 Introduction

While conventional photodetectors can only measure light intensity, the light field contains much richer information, including but not limited to phase, polarization, and spectrum. The measurement of multi-dimensional light field information can find its application in various fields. For instance, polarization measurements can reveal the material composition [1, 2] and surface textures [3] of objects, whereas spectral analysis can be instrumental for chemical study [4] and wavelength-division-based telecommunication [5].

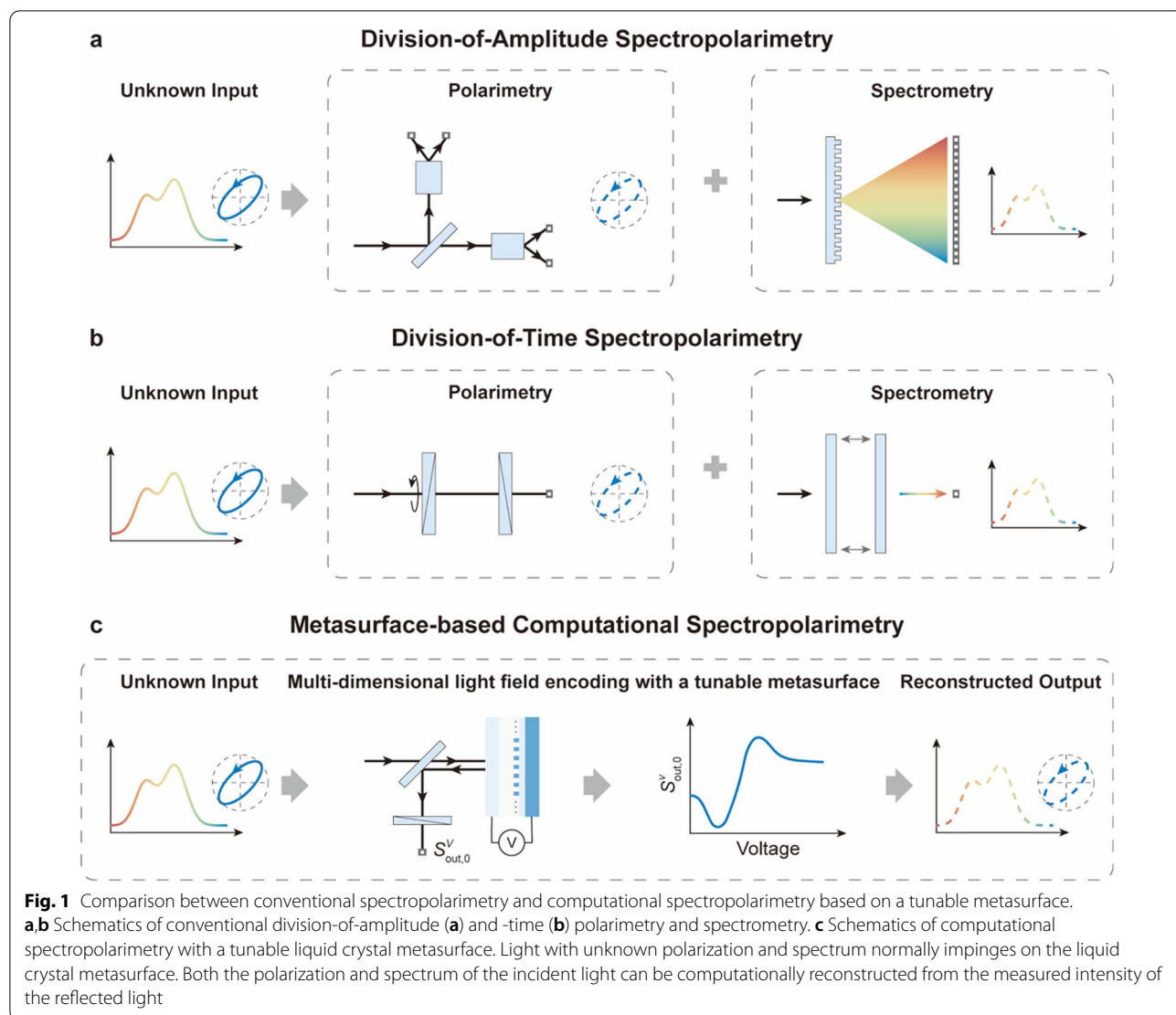
However, conventional polarimeters and spectrometers are often bulky [6, 7], which hinders their applications in miniaturized platforms. Division-of-amplitude polarimeters and spectrometers utilize polarization beam splitters and dispersive elements, such as prisms and gratings, to spatially separate and distinguish light with different

polarization and wavelength, as schematically shown in Fig. 1a. Alternatively, division-of-time polarimeters and spectrometers leverage tunable polarization and wavelength filters to sequentially measure the light intensity with different polarization and spectral components, as schematically shown in Fig. 1b. Through the multiplexing of the abovementioned mechanisms for polarization and spectrum detection, composite systems that can simultaneously measure the polarization and spectrum of light, namely spectropolarimeter, have been developed recently. However, the multiplexing inevitably results in a further increased system form factor and complexity [8–10].

Metasurface is an emerging class of planar diffractive optical elements. Its design flexibility has broken new ground for manipulating the vectorial light field [11–17]. In recent years, metasurface-based polarimeters and spectrometers have also been developed. Besides conventional approaches based on either division-of-amplitude [18–23] or division-of-time [24, 25], computational polarimeters and spectrometers have recently been demonstrated, in which the polarization or spectrum of the

\*Correspondence: ymyang@tsinghua.edu.cn

State Key Laboratory of Precision Measurement Technology and Instruments, Department of Precision Instrument, Tsinghua University, Beijing 100084, China



incident light can be encoded using a tunable graphene-integrated metasurface [26] or a metasurface array [27–30], and decoded through computational reconstruction. However, the simultaneous multiplexing and reconstruction of multi-dimensional light field information remain a challenging task. Alternatively, metasurface-based spectropolarimetry has been demonstrated by spatially splitting the incident light with different polarization components and wavelengths [31–33]. However, similar to conventional division-of-amplitude polarimeters and spectrometers, such an approach requires a detector array for polarization and spectrum detection at a single spatial location, thus preventing its use for spectropolarimetric imaging.

In this work, we propose and experimentally demonstrate a spectropolarimeter that simultaneously measures the polarization and spectrum of near-infrared light. The core hardware part of the system is an electrically-tunable liquid crystal-embedded silicon metasurface. The metasurface is tailored to support multiple high-quality-factor guided-mode resonances, with rich and anisotropic spectral features that can be widely tuned by applying different bias voltages. Combined with a straightforward computational reconstruction algorithm based on the trust-region method [34], the system can reconstruct the incident light’s full Stokes parameters and spectrum from the reflected light intensity recorded by a single-pixel photodetector. Unlike conventional spectropolarimetry,

the proposed method does not perturb the wavefront of the incident light. The fabrication of the liquid crystal metasurface is fully compatible with the mature complementary metal-oxide semiconductor (CMOS) and liquid crystal on silicon (LCoS) manufacturing process, such that the system may be mass produced at a low cost.

## 2 Results

### 2.1 Working principle of tunable metasurface-based spectropolarimetry

The working principle of the tunable liquid crystal metasurface-based computational spectropolarimeter is schematically shown in Fig. 1c. We first consider incident light with unknown polarization and spectrum, described by a wavelength-dependent Stokes vector  $S_{\text{in}}(\lambda) = [s_0(\lambda) \ s_1(\lambda) \ s_2(\lambda) \ s_3(\lambda)]^T$ . To measure  $S_{\text{in}}(\lambda)$ , the incident light field is designed to pass through and be encoded by a liquid crystal metasurface, a polarizer, and eventually be detected by a photodetector. The polarizer is added between the metasurface and the photodetector to enable the measurement system to detect circularly polarized light. The modulated Stokes vector  $S_{\text{out}}(\lambda) = \mathbf{M}(\lambda, V) \cdot S_{\text{in}}(\lambda)$ , where  $\mathbf{M}(\lambda, V)$  is a  $4 \times 4$  Mueller matrix of the measurement system, which is a function of the wavelength  $\lambda$  as well as the voltage  $V$  applied to the liquid crystal metasurface.  $\mathbf{M}(\lambda, V) = \mathbf{M}_p \cdot \mathbf{M}_{\text{meta}}(\lambda, V)$ , where  $\mathbf{M}_p$  and  $\mathbf{M}_{\text{meta}}(\lambda, V)$  are Mueller matrices of the polarizer and metasurface, respectively.

Since a photodetector can only record the light intensity, which corresponds to the element  $s_0$  in  $S_{\text{out}}(\lambda)$ , the detected light intensity can be written as,

$$s_{\text{out},0} = M_0 \cdot S_{\text{in}} \quad (1)$$

where  $M_0 = [m_{00} \ m_{01} \ m_{02} \ m_{03}]$  is the first row of  $\mathbf{M}(\lambda, V)$ . For broadband incident light, by sequentially altering the voltage applied to the liquid crystal metasurface, its polarization and spectrum are encoded in the measured light intensity as,

$$S_{\text{out},0}^V = \sum_{i=1}^m a_i \mathbf{M}_0^V(\lambda_i) S_{\text{in}}(\lambda_i) \quad (2)$$

where  $S_{\text{out},0}^V$  is an  $N \times 1$  vector, corresponding to the intensity measured at  $N$  different voltages;  $m$  is the

number of spectral channels;  $a_i$  represents the weight of each spectral channel.  $\mathbf{M}_0^V(\lambda_i)$  is an  $N \times 4$  matrix with the form of  $[M_0(\lambda_i, V_1) \ M_0(\lambda_i, V_2) \ \dots \ M_0(\lambda_i, V_N)]^T$ . With a pre-calibrated  $\mathbf{M}_0^V(\lambda)$ , it is possible to simultaneously reconstruct the polarization and spectrum of the incident light by fitting the measured intensity according to Eq. (2). Depending on the number of unknown parameters, it may be an underdetermined or overdetermined nonlinear least squares problem and can be solved with many well-developed methods, such as the Gauss–Newton method and the trust-region method [34].

### 2.2 Design of the liquid crystal metasurface

To ensure the fidelity of the polarization and wavelength reconstruction, the measurement matrix  $\mathbf{M}_0^V(\lambda)$  at different values of  $\lambda$  should have a minimal correlation [27, 28, 35], which demands the metasurface to exhibit rich spectral and polarization features that can be widely tuned by an applied voltage.

The proposed metasurface is a one-dimensional 500-nm-thick silicon grating. The metasurface is embedded in liquid crystal and further covered with a transparent indium-tin-oxide (ITO) electrode for active modulation, as schematically shown in Fig. 2a. The metasurface is designed to be highly anisotropic and supports multiple high-Q guided-mode resonances (Additional file 1: Note S1). While the director of the liquid crystal is along the  $y$ -axis in the static case, when an alternating voltage is applied to the liquid crystal cell, the liquid crystal director rotates towards the  $z$ -axis, giving rise to a change of the liquid crystal's refractive index along both the  $y$ -axis and  $z$ -axis and a spectral shift of the guided-mode resonances. The reflectance and reflection phase of the metasurface vary strongly as a function of the liquid crystal rotation angle (denoted by  $\theta_{\text{LC}}$ ) for incident light polarized both along the  $x$ -axis and  $y$ -axis, are shown in Fig. 2b–e, which is also a result of the strong modal overlap between the liquid crystal and the guided-mode resonances, as shown in Fig. 2f,g.

### 2.3 Numerical simulation

To numerically validate the tunable liquid crystal metasurface for spectropolarimetry, we first calculate the

(See figure on next page.)

**Fig. 2** Liquid crystal metasurface design. **a** Schematics of the liquid crystal metasurface. The grating period  $P = 950$  nm, bar width  $W = 160$  nm, and bar height  $H_1 = 500$  nm. The thickness of the liquid crystal layer  $H_2 = 2.5$   $\mu\text{m}$ . **b,c** Simulated reflectance of the metasurface as a function of the liquid crystal rotation angle  $\theta_{\text{LC}}$  for incident light polarized along the  $x$ -axis (**b**) and  $y$ -axis (**c**), respectively. **d,e** Simulated reflection phase of the metasurface as a function of the liquid crystal rotation angle  $\theta_{\text{LC}}$  for incident light polarized along the  $x$ -axis (**d**) and  $y$ -axis (**e**), respectively. **f** Simulated  $z$ -component electric field distribution for incident light polarized along the  $x$ -axis at the wavelength of 1452 nm with  $\theta_{\text{LC}} = 0^\circ$ , corresponding to the black star in panel (**b**). **g** Simulated  $z$ -component magnetic field distribution for incident light polarized along the  $y$ -axis at the wavelength of 1479 nm with  $\theta_{\text{LC}} = 45^\circ$ , corresponding to the black triangle in panel (**c**)

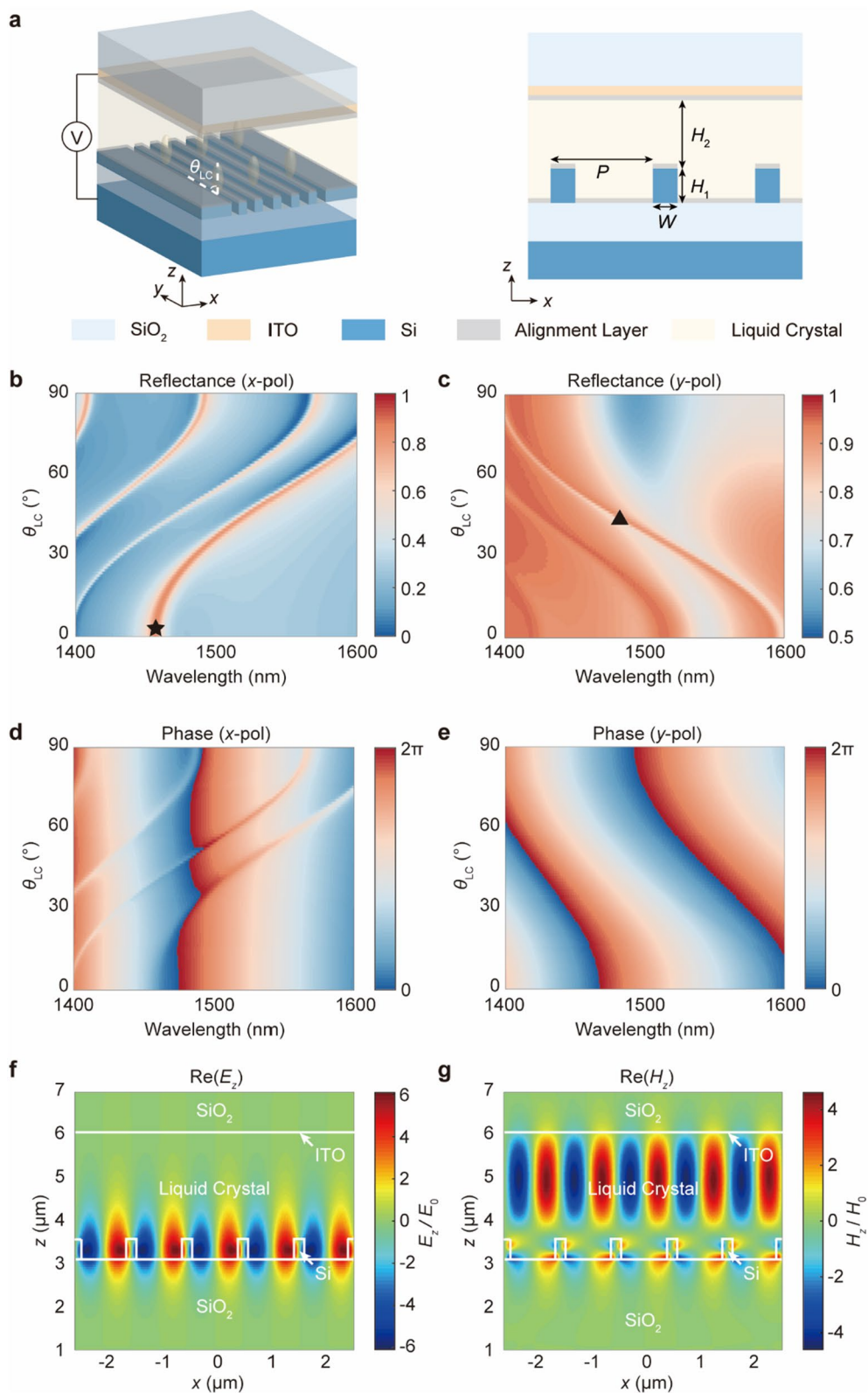


**Fig. 2** (See legend on previous page.)



elements in  $M_0$  at each  $\lambda$  and  $\theta_{LC}$  from the simulated complex amplitude reflection of the metasurface as,

$$\begin{aligned} m_{00} &= \frac{1}{2}(|r_x|^2 \cos^2 \theta_p + |r_y|^2 \sin^2 \theta_p) \\ m_{01} &= \frac{1}{2}(|r_x|^2 \cos^2 \theta_p - |r_y|^2 \sin^2 \theta_p) \\ m_{02} &= \frac{1}{2}|r_x||r_y| \sin(2\theta_p) \cos(\Delta\varphi) \\ m_{03} &= \frac{1}{2}|r_x||r_y| \sin(2\theta_p) \sin(\Delta\varphi) \end{aligned} \quad (3)$$

where  $r_x$  and  $r_y$  represent the complex amplitude of  $x$ - and  $y$ -polarized light reflected from the metasurface, respectively.  $\theta_p$  is the polarizer's transmission axis with respect to the  $x$ -axis, and  $\Delta\varphi = \arg(r_x) - \arg(r_y)$ . (Additional file 1: Note S2).

To quantify the diversity of the spectral response of the liquid crystal metasurface, we calculate correlation coefficients of each column of the Mueller matrix at different wavelengths (Additional file 1: Note S3). The calculated correlation coefficients of the Mueller matrix are relatively small for the wavelength range from 1400 to 1500 nm, suggesting superior spectral diversity required for high-fidelity spectral reconstruction.

To numerically verify the effectiveness of the proposed tunable metasurface for polarization and wavelength measurement of the monochromatic incident light, we assume three random incident wavelengths within the range from 1400 to 1500 nm and three representative incident polarization states (linearly polarized, left-elliptically polarized, and right-circularly polarized, respectively). To simulate the inevitable noise sources in experiments, random noise with a maximum signal-to-noise ratio ( $SNR$ ) of 10 dB, defined as  $SNR = -10 \lg \frac{I_n}{I_s}$ , where  $I_n$  and  $I_s$  represent the intensity of noise and signal, respectively, is added to the calculated reflectance. To reconstruct the polarization state and wavelength, we take the Stokes parameters  $S_{in}$  and  $\lambda$  as variables and fit the relationship between

the reflectance and  $\theta_{LC}$  to Eq. (1), with the number of measurements  $N_p$  set to 10. For the computational reconstruction, we choose the trust-region method because of its reasonably low computational cost and superior global convergence properties [34]. The reconstructed polarization and wavelengths of the incident light show excellent agreement with the ground truths, as illustrated in Fig. 3a.

The fidelity of the reconstruction is related to  $N_p$  and  $SNR$  of the measured reflected light intensity. We define the polarization reconstruction error as  $\varepsilon_p = \arccos(\frac{S_1 S'_1 + S_2 S'_2 + S_3 S'_3}{S_0 S'_0})$ , which corresponds to the angle between the ground truth and the reconstructed point on the Poincaré sphere, as illustrated in Fig. 3b, where  $[S'_0 \ S'_1 \ S'_2 \ S'_3]^T$  is the reconstructed Stokes vector. The wavelength reconstruction error is defined as  $\varepsilon_\lambda = \left| \lambda - \lambda' \right| / \lambda$ , where  $\lambda'$  is the reconstructed wavelength.

We evaluate  $\varepsilon_p$  and  $\varepsilon_\lambda$  by randomly assuming incident polarization states over the full range of the Poincaré sphere and incident wavelengths ranging from 1400 to 1500 nm.  $\varepsilon_p$  and  $\varepsilon_\lambda$  as a function of  $N_p$  at a fixed  $SNR$  of 10 dB and as a function of the  $SNR$  at a fixed  $N_p$  of 20 are shown in Fig. 3c,d, respectively. The results indicate that the metasurface-based spectropolarimeter may reconstruct the polarization state and wavelength of monochromatic light with high fidelity ( $\varepsilon_p < 5^\circ$  and  $\varepsilon_\lambda < 0.5\%$ ) at relatively high noise level using no more than 10 measurements.

To further validate the effectiveness of the tunable liquid crystal metasurface for broadband spectropolarimetric measurement, a broadband light source with a spectral range from 1420 to 1480 nm and a sampling interval of 1 nm is assumed as the incident light. Random noise with a maximum  $SNR$  of 20 dB is added to the calculated reflectance. The number of measurements  $N_p$  is set to 90 to make the reconstruction process an over-determined problem to lessen the influence of the noise. The reconstructed polarization and spectrum are also

(See figure on next page.)

**Fig. 3** Simulated spectropolarimetric reconstruction. **a** Comparison of reconstructed wavelengths and polarization states with the ground truth for monochromatic incident light. Dashed and solid lines in insets represent reconstructed polarization states and ground truth, respectively. **b** Illustration of the Poincaré sphere and the definition of  $\varepsilon_p$ . The solid and hollow circle represents the ground truth and reconstructed polarization, respectively. **c,d** The polarization and wavelength measurement error  $\varepsilon_p$  (blue line) and  $\varepsilon_\lambda$  (orange line) as a function of  $N_p$  (**c**) and  $SNR$  (**d**), respectively. **e** Comparison between the reconstructed spectrum (upper panel) and Stokes parameters (lower panel) and the ground truth for a broadband input signal. Dashed and solid lines in the inset of the upper panel represent reconstructed polarization states and the ground truth, respectively. **f** Reconstructed narrowband spectra with a fixed bandwidth of 2 nm and peak positions of 1430 nm, 1450 nm, and 1470 nm, respectively. Dashed and solid lines in the inset represent reconstructed polarization states and the ground truth, respectively. **g** Reconstructed peak positions of narrowband spectra ranging from 1400 to 1500 nm with a fixed bandwidth of 2 nm. The solid line is the mean reconstructed peak positions over different reconstruction cycles. The upper and lower boundaries of the shaded region are the corresponding standard deviations of the reconstructed peak position. **h** Reconstructed bandwidths of spectra with a fixed peak position of 1455 nm and bandwidths ranging from 1 to 10 nm. The blue line is the mean reconstructed bandwidths over different reconstruction cycles, and the black line is the ground truth. The upper and lower boundaries of the shaded region are the corresponding standard deviations of the reconstructed bandwidth

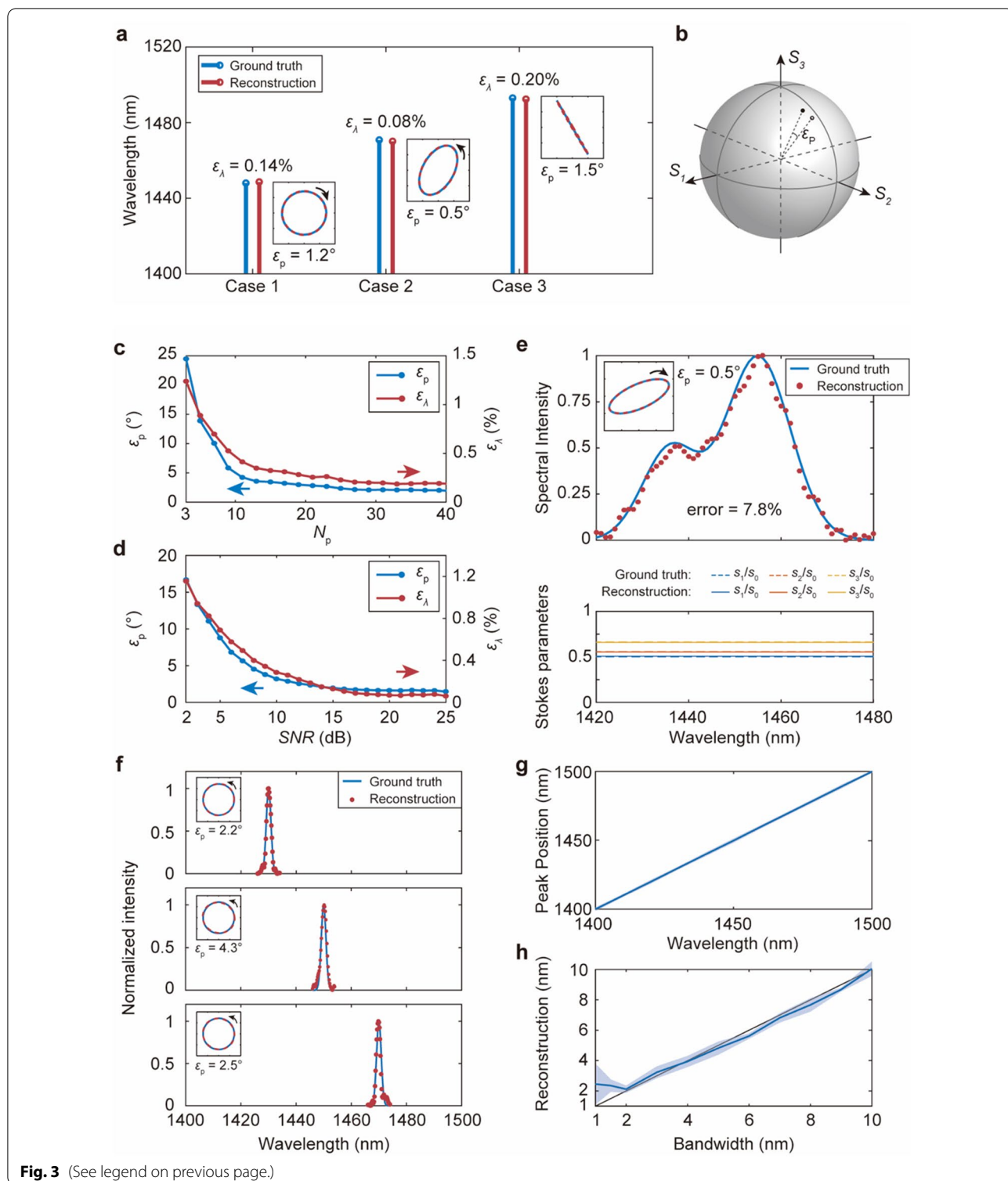


**Fig. 3** (See legend on previous page.)

compared with the ground truth, as shown in Fig. 3e. The spectrum reconstruction error here is calculated by  $\|I_0 - I_R\|_1 / \|I_0\|_1$ , where  $I_0$  and  $I_R$  are the ground truth and the reconstructed spectrum, respectively. While the

polarization reconstruction result agrees very well with the ground truth, the spectrum reconstruction error is higher than that in the monochromatic case.

To test the resolution limit, we performed the reconstruction of a left-circularly polarized narrowband signal with a spectral peak position ranging from 1400 to 1500 nm and with a tunable bandwidth ranging from 1 to 10 nm. A few representative reconstruction results of narrowband spectra with varying peak positions with a bandwidth of 2 nm are shown in Fig. 3f. The reconstructed peak positions agree well with the ground truth across the full wavelength range from 1400 to 1500 nm, as shown in Fig. 3g. Furthermore, with the spectral peak position fixed at 1455 nm, the reconstructed bandwidth matches well with the ground truth with the bandwidth down to about 2 nm, as shown in Fig. 3h.

Here, the spectral resolution is limited by the correlation of the spectral response of the metasurface as well as the noise level. By designing guided-mode resonances with higher Q-factors, one may be able to further reduce the spectral correlation of the measurement matrix, allowing the reconstruction of a narrower spectrum.

## 2.4 Experimental demonstration

For the experimental demonstration of the liquid crystal metasurface spectropolarimetry, we fabricate the metasurface via the standard electron beam lithography and reactive ion etching process. The liquid crystal cell packaging also follows a procedure routinely used for liquid crystal devices (Additional file 1: Note S4). The photograph and the scanning electron microscopy (SEM) image of the metasurface are shown in Fig. 4a.

Prior to the spectropolarimetric measurement, we calibrated  $\mathbf{M}_0^V(\lambda)$  of the fabricated metasurface at each wavelength. The experimental setup for both the calibration and measurement processes is shown in Fig. 4b (Additional file 1: Note S5). We first set the incident light to a known polarization, then rotate the polarizer to collect a set of output intensity  $S_{\text{out},0}(\lambda, V, \theta_p)$  at each value of  $V$  and  $\lambda$ . By fitting the intensity to Eqs. (1) and (3),  $r_x$ ,  $r_y$ , and  $\Delta\phi$  as functions of  $V$  and  $\lambda$  can be obtained, as shown in Fig. 4c.  $\mathbf{M}_0^V(\lambda)$  can be subsequently obtained from Eq. (3). The wavelength range of the experimental calibration is from 1420 to 1470 nm, beyond which the spectral correlation of the measured Mueller matrix becomes too

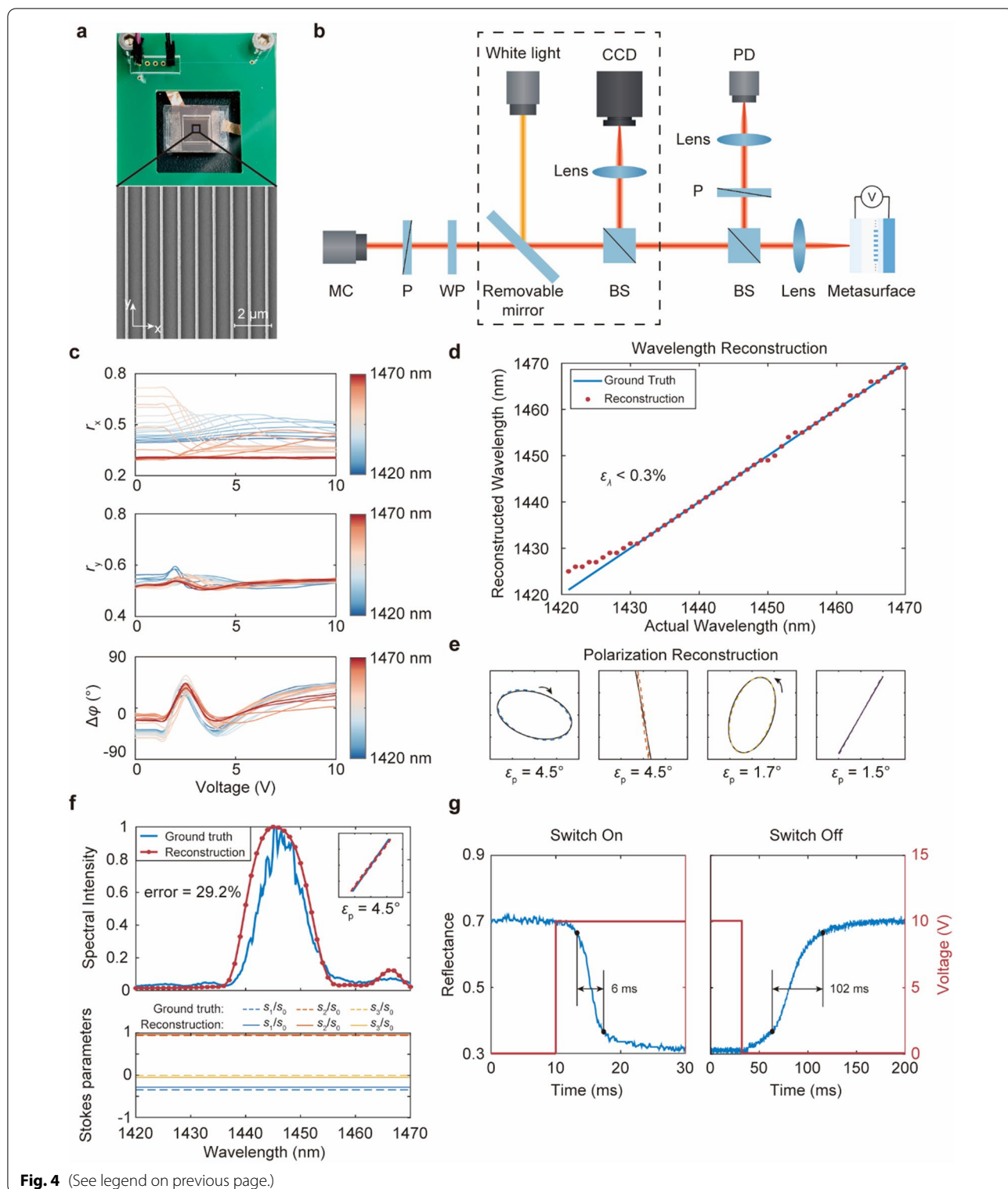
large. Besides a clear main guided-mode resonance peak, a few other simulated guided-mode resonances were not experimentally observed, which may be due to the inhomogeneous liquid crystal alignment and imperfect fabrication (Additional file 1: Note 6).

To experimentally demonstrate the simultaneous reconstruction of the polarization and wavelength of a monochromatic light using the tunable metasurface, we varied the wavelength of the incident light from 1420 to 1470 nm, with its polarization state prepared as linear or elliptical. In the measurement system,  $\theta_p$  was fixed at  $45^\circ$  to minimize the condition number of the system matrix (Additional file 1: Note S7). For each input wavelength and polarization, a set of reflectance was measured by sweeping the voltage applied to the liquid crystal metasurface. By fitting the measured reflectance to Eq. (1) using the trust-region method, the wavelength and polarization of the incident light can be simultaneously reconstructed and are in good agreement with the ground truth, as shown in Fig. 4d, e.

To characterize the spectral resolution of the spectropolarimetric measurement system, we performed reconstruction of a linearly polarized narrowband light source (with a bandwidth of about 9 nm) generated from a supercontinuum laser source coupled to an acousto-optic tunable filter. The experimental reconstruction result, as shown in Fig. 4f, demonstrates that we can reconstruct the spectral peak location, the overall spectral line shape, as well as its polarization state. Based on the experimentally measured Mueller matrix, we also numerically reconstructed an unknown input light source with a dual-peak spectrum (Additional file 1: Supplementary note S8). The lower experimental spectral resolution can be anticipated as a result of the relatively strong spectral correlation of the experimental Mueller matrix. The fidelity of the broadband spectrum reconstruction may be further improved by reducing the system noise, improving the refractive index modulation range, the Q-factor of the guided-mode resonances, as well as its modal overlap with the liquid crystal.

(See figure on next page.)

**Fig. 4** Experimental spectropolarimetric reconstruction. **a** Photograph (upper panel) and SEM image (lower panel) of the fabricated liquid crystal metasurface. **b** Experimental setup for the Mueller matrix calibration and spectropolarimetric measurements. **c** Calibrated  $r_x$ ,  $r_y$ , and  $\Delta\phi$  as functions of  $V$  in the wavelength range from 1420 to 1470 nm. **d** Comparison of reconstructed wavelengths (orange dots) of monochromatic incident light (from 1420 to 1470 nm, with 1 nm separation) with the ground truth (blue line). **e** Comparison of reconstructed polarization states (dashed lines) of monochromatic incident light and the ground truth (solid lines). **f** Comparison between the experimentally reconstructed spectrum (upper panel) and Stokes parameters (lower panel) and the ground truth for a narrowband input signal. Dashed and solid lines in the inset of the upper panel represent the reconstructed polarization state and the ground truth, respectively. **g** Experimentally measured switch-on and switch-off time of the liquid crystal metasurface, respectively. Blue and red lines represent the measured reflectance and the voltage applied to the metasurface as a function of time, respectively



To characterize the operation speed of the proposed spectropolarimetry, we experimentally measured the response time of the tunable liquid crystal metasurface

with a 10-V-voltage switched on and off. The response time is defined as the time between 10 and 90% of the reflectance change. As shown in Fig. 4g, the switch-on



and switch-off time are 6 ms and 102 ms, respectively. For each spectropolarimetric measurement, the applied voltage is sequentially swept from 0 to 10 V, leading to a total measurement time of 60 ms with 10 measurements. The response time of the liquid crystal may be further shortened by reducing the cell gap [36–39]. The subsequent computational reconstruction is performed in MATLAB and takes about 300 ms on a desktop computer with an Intel i5-8500 CPU and 32 GB RAM. The speed and accuracy of the spectropolarimetric reconstruction may be further improved through the use of data-driven deep learning-based algorithms [29, 40].

### 3 Discussion and conclusion

To summarize, we have demonstrated a tunable metasurface-based multi-dimensional light field encoder that allows the simultaneous measurement of the polarization and spectrum of near-infrared light. The metasurface encodes the polarization and spectral information using its anisotropic high-Q guided-mode resonances that can be tuned by a bias voltage. Although the liquid crystal metasurface currently operates in the reflection mode, one can also design a transmissive liquid crystal metasurface [41–45] to enable more compact integration with the photodetector (Additional file 1: Supplementary note S9). Due to its in-plane uniformity, the liquid crystal metasurface does not perturb the wavefront of the incident light. Compared with division-of-amplitude-based spectropolarimetric measurement techniques, the liquid crystal metasurface, when integrated with a proper detector array, may be used for spectropolarimetric imaging without sacrificing spatial resolution (Additional file 1: Supplementary note S10). With the adoption of widely-used liquid crystal material and cell assembly process, the response of the liquid crystal metasurface is repeatable under different operation cycles (Additional file 1: Note S11). The reflectance, and consequently the *SNR*, of the measurement system may be further increased by taking it into consideration during the design stage of the metasurface. The measurement time may be further reduced by reducing the cell gap and employing more advanced reconstruction algorithms, thus allowing spectropolarimetric imaging with a much higher frame rate. The proposed liquid crystal metasurface may be used in a plethora of applications that require polarization and spectral measurements, such as in biomedical imaging, remote sensing, and optical communication. Such a strategy may also be extended to construct compact systems that can measure additional light field information, such as the depth of a target scene or the wavefront of the incident light.

### Abbreviations

CMOS: Complementary metal-oxide semiconductor; LCoS: Liquid crystal on silicon; ITO: Indium-tin-oxide; SNR: Signal-to-noise ratio; SEM: Scanning electron microscopy.

### Supplementary Information

The online version contains supplementary material available at <https://doi.org/10.1186/s43593-022-00032-0>.

**Additional file 1: Figure S1.** Calculated correlation coefficients of the Mueller matrix  $c_{00}$ ,  $c_{01}$ ,  $c_{02}$ , and  $c_{03}$  over the wavelength range from 1300 nm to 1600 nm. **Figure S2.** The experimentally measured reflectance for incident light polarized along the  $x$ -axis as a function of the voltage applied to the metasurface. **Figure S3.** Calculated condition number  $\kappa$  of the measurement matrix  $\mathbf{M}_0^V(\lambda)$  as a function of  $\theta_p$ . **Figure S4.** Spectropolarimetric reconstruction results of dual-peak spectra. **Figure S5.** Transmissive liquid crystal metasurface design with numerical spectropolarimetric reconstruction results. **Figure S6.** Possible schematic of a liquid crystal metasurface-based spectropolarimetric imaging system. **Figure S7.** Measured voltage-dependent reflectance of the liquid crystal metasurface.

### Acknowledgements

The authors acknowledge Dr. Qing Hu at Ning-Cui Optics Inc. for assembling the liquid crystal cell with the metasurface.

### Author contributions

YN designed and characterized the metasurface and developed the spectropolarimetric reconstruction algorithm with assistance from CC, SW, and XX; all authors analyzed the data; YN and YY prepared the manuscript with input from all authors; YY initialized and supervised the project. All authors read and approved the final manuscript.

### Funding

This work was supported by the National Natural Science Foundation of China (61975251, 62135008) and by the Guoqiang Institute, Tsinghua University.

### Availability of data and materials

The datasets used and/or analyzed during the current study are available from the corresponding author on reasonable request.

### Declarations

#### Competing interests

The authors declare that they have no competing interests.

Received: 4 August 2022 Revised: 15 September 2022 Accepted: 19 September 2022

Published online: 04 November 2022

### References

1. C. He, H. He, J. Chang, B. Chen, H. Ma, M.J. Booth, Polarisation optics for biomedical and clinical applications: a review. *Light Sci. Appl.* **10**, 194 (2021)
2. H. Zhang, Z. Ni, C.E. Stevens, A. Bai, F. Peiris, J.R. Hendrickson, L. Wu, D. Jariwala, Cavity-enhanced linear dichroism in a Van Der Waals antiferromagnet. *Nat. Photonics* **16**, 311–317 (2022)
3. J.S. Tyo, D.L. Goldstein, D.B. Chenault, J.A. Shaw, Review of passive imaging polarimetry for remote sensing applications. *Appl. Opt.* **45**, 5453–5469 (2006)
4. H.W. Thompson, Infra-Red spectroscopy and chemical industry. *Nature* **177**, 915–917 (1956)

5. X.G. Zhang, Y.L. Sun, B. Zhu, W.X. Jiang, Q. Yu, H.W. Tian, C.-W. Qiu, Z. Zhang, T.J. Cui, A metasurface-based light-to-microwave transmitter for hybrid wireless communications. *Light Sci. Appl.* **11**, 126 (2022)
6. H.G. Berry, G. Gabrielse, A.E. Livingston, Measurement of the Stokes parameters of light. *Appl. Opt.* **16**, 3200–3205 (1977)
7. W.W. Parson, *Modern optical spectroscopy* (Springer, Berlin, 2007)
8. S. Frans, H.H.R. Jeroen, H. Gerard, M.S. Daphne, U.K. Christoph, J.M. Smit, C.L. Erik, L.V. Ad, H. Rik ter, N. Ramón, W. Klaas, G.M. Scott, V. Robert, SPEX: the spectropolarimeter for planetary exploration. *Proc. SPIE*. **7731**, 77311B (2010)
9. M.F. Sterzik, S. Bagnulo, E. Palle, Biosignatures as revealed by spectropolarimetry of Earthshine. *Nature* **483**, 64–66 (2012)
10. F. Iglesias, A. Feller, Instrumentation for solar spectropolarimetry: state of the art and prospects. *Opt. Eng.* **58**, 082417 (2019)
11. N. Yu, P. Genevet, M.A. Kats, F. Aieta, J.-P. Tetienne, F. Capasso, Z. Gaburro, Light propagation with phase discontinuities: generalized laws of reflection and refraction. *Science* **334**, 333–337 (2011)
12. D. Lin, P. Fan, E. Hasman, M.L. Brongersma, Dielectric gradient metasurface optical elements. *Science* **345**, 298–302 (2014)
13. Y. Yang, W. Wang, P. Moitra, I.I. Kravchenko, D.P. Briggs, J. Valentine, Dielectric meta-reflectorarray for broadband linear polarization conversion and optical vortex generation. *Nano Lett.* **14**, 1394–1399 (2014)
14. A. Arbabi, Y. Horie, M. Bagheri, A. Faraon, Dielectric metasurfaces for complete control of phase and polarization with subwavelength spatial resolution and high transmission. *Nat. Nanotechnol.* **10**, 937–943 (2015)
15. Y. Ni, S. Chen, Y. Wang, Q. Tan, S. Xiao, Y. Yang, Metasurface for structured light projection over 120 degrees field of view. *Nano Lett.* **20**, 6719–6724 (2020)
16. F. Zhao, R. Lu, X. Chen, C. Jin, S. Chen, Z. Shen, C. Zhang, Y. Yang, Metalens-Assisted System for Underwater Imaging. *Laser Photonics Rev.* **15**, 2100097 (2021)
17. L. Li, H. Zhao, C. Liu, L. Li, T.J. Cui, Intelligent metasurfaces: control, communication and computing. *eLight* **2**, 7 (2022)
18. J.P. Balthasar Mueller, K. Leosson, F. Capasso, Ultracompact metasurface in-line polarimeter. *Optica* **3**, 42–47 (2016)
19. E. Arbabi, S.M. Kamali, A. Arbabi, A. Faraon, Full-stokes imaging polarimetry using dielectric metasurfaces. *ACS Photonics* **5**, 3132–3140 (2018)
20. A. Tittl, A. Leitis, M. Liu, F. Yesilkoy, D.Y. Choi, D.N. Neshev, Y.S. Kivshar, H. Altug, Imaging-based molecular barcoding with pixelated dielectric metasurfaces. *Science* **360**, 1105–1109 (2018)
21. N.A. Rubin, G. D'Aversa, P. Chevalier, Z. Shi, W.T. Chen, F. Capasso, Matrix Fourier optics enables a compact full-stokes polarization camera. *Science* **365**, eaax1839 (2019)
22. A. Basiri, X. Chen, J. Bai, P. Amrollahi, J. Carpenter, Z. Holman, C. Wang, Y. Yao, Nature-inspired chiral metasurfaces for circular polarization detection and full-stokes polarimetric measurements. *Light Sci. Appl.* **8**, 78 (2019)
23. J. Wei, Y. Li, L. Wang, W. Liao, B. Dong, C. Xu, C. Zhu, K.W. Ang, C.W. Qiu, C. Lee, Zero-bias mid-infrared graphene photodetectors with bulk photoreponse and calibration-free polarization detection. *Nat. Commun.* **11**, 6404 (2020)
24. A.S.P. Chang, K.J. Morton, H. Tan, P.F. Murphy, W. Wu, S.Y. Chou, Tunable liquid crystal-resonant grating filter fabricated by nanoimprint lithography. *IEEE Photon. Technol. Lett.* **19**, 1457–1459 (2007)
25. M.N. Julian, C. Williams, S. Borg, S. Bartram, H.J. Kim, Reversible optical tuning of GeSbTe phase-change metasurface spectral filters for mid-wave infrared imaging. *Optica* **7**, 746–754 (2020)
26. M. Jung, S. Dutta-Gupta, N. Dabidian, I. Brener, M. Shcherbakov, G. Shvets, Polarimetry using graphene-integrated anisotropic metasurfaces. *ACS Photonics* **5**, 4283–4288 (2018)
27. Z. Wang, S. Yi, A. Chen, M. Zhou, T.S. Luk, A. James, J. Nogan, W. Ross, G. Joe, A. Shahsafi, K.X. Wang, M.A. Kats, Z. Yu, Single-shot on-chip spectral sensors based on photonic crystal slabs. *Nat. Commun.* **10**, 1020 (2019)
28. Y. Zhu, X. Lei, K.X. Wang, Z. Yu, Compact CMOS spectral sensor for the visible spectrum. *Photon. Res.* **7**, 961–966 (2019)
29. W. Zhang, H. Song, X. He, L. Huang, X. Zhang, J. Zheng, W. Shen, X. Hao, X. Liu, Deeply learned broadband encoding stochastic hyperspectral imaging. *Light Sci. Appl.* **10**, 108 (2021)
30. J. Xiong, X. Cai, K. Cui, Y. Huang, J. Yang, H. Zhu, W. Li, B. Hong, S. Rao, Z. Zheng, S. Xu, Y. He, F. Liu, X. Feng, W. Zhang, Dynamic brain spectrum acquired by a real-time ultraspectral imaging chip with reconfigurable metasurfaces. *Optica* **9**, 461–468 (2022)
31. E. Maguid, I. Yulevich, D. Veksler, V. Kleiner, L. Brongersma, E. Hasman, Photonic spin-controlled multifunctional shared-aperture antenna array. *Science* **352**, 1202–1206 (2016)
32. W.T. Chen, P. Török, M.R. Foreman, C.Y. Liao, W.-Y. Tsai, P.R. Wu, D.P. Tsai, Integrated plasmonic metasurfaces for spectropolarimetry. *Nanotechnology* **27**, 224002 (2016)
33. F. Ding, A. Pors, Y.T. Chen, V.A. Zenin, S.I. Bozhevolnyi, Beam-size-invariant spectropolarimeters using gap-plasmon metasurfaces. *ACS Photonics* **4**, 943–949 (2017)
34. J. Nocedal, S.J. Wright, *Numerical optimization* (Springer, Berlin, 1999)
35. U. Kurokawa, B.I. Choi, C. Chang, Filter-based miniature spectrometers: spectrum reconstruction using adaptive regularization. *IEEE Sens. J.* **11**, 1556–1563 (2011)
36. H. Wang, Studies of liquid crystal response time. University of Central Florida, 2005.
37. G.M. Akselrod, Y. Yang, P. Bowen, Tunable liquid crystal metasurfaces. U.S. Patent 10,665,953 B1, 24 Sept 2020.
38. J. Xiong, S.-T. Wu, Planar liquid crystal polarization optics for augmented reality and virtual reality: from fundamentals to applications. *eLight* **1**, 3 (2021)
39. S. Mansha, P. Moitra, X. Xu, T.W.W. Mass, R.M. Veetil, X. Liang, S.-Q. Li, R. Paniagua-Domínguez, A.I. Kuznetsov, High resolution multispectral spatial light modulators based on tunable Fabry-Perot nanocavities. *Light Sci. Appl.* **11**, 141 (2022)
40. Y. LeCun, Y. Bengio, G. Hinton, Deep learning. *Nature* **521**, 436–444 (2015)
41. A. Komar, R. Paniagua-Domínguez, A. Miroshnichenko, Y.F. Yu, Y.S. Kivshar, A.I. Kuznetsov, D. Neshev, Dynamic beam switching by liquid crystal tunable dielectric metasurfaces. *ACS Photonics* **5**, 1742–1748 (2018)
42. S.-Q. Li, X. Xu, R. Maruthiyodan Veetil, V. Valuckas, R. Paniagua-Domínguez, A.I. Kuznetsov, Phase-only transmissive spatial light modulator based on tunable dielectric metasurface. *Science* **364**, 1087 (2019)
43. Z. Shen, S. Zhou, X. Li, S. Ge, P. Chen, W. Hu, Y. Lu, Liquid crystal integrated metalens with tunable chromatic aberration. *Adv. Photon.* **2**, 036002 (2020)
44. I. Kim, M.A. Ansari, M.Q. Mehmood, W.-S. Kim, J. Jang, M. Zubair, Y.-K. Kim, J. Rho, Stimuli-responsive dynamic metaholographic displays with designer liquid crystal modulators. *Adv. Mater.* **32**, 2004664 (2020)
45. Y. Hu, X. Ou, T. Zeng, J. Lai, J. Zhang, X. Li, X. Luo, L. Li, F. Fan, H. Duan, Electrically tunable multifunctional polarization-dependent metasurfaces integrated with liquid crystals in the visible region. *Nano Lett.* **21**, 4554–4562 (2021)